PCCP

Boosting the activity of transition metal carbides towards methane activation by nanostructuring

Journal:	*Physical Chemistry Chemical Physics*
Manuscript ID	CP-ART-01-2020-000228.R2
Article Type:	Paper
Date Submitted by the Author:	12-Mar-2020
Complete List of Authors:	Figueras, Marc; Universitat de Barcelona, Departament de Ciència de Materials i Química Física & IQTCUB Gutierrez, Ramon ; Universidad Central de Venezuela, Facultad de Ciencias Prats, Héctor; Universitat de Barcelona, Departament de Quimica Fisica & IQTCUB Viñes, Francesc; University of Barcelona, Physical Chemistry Ramirez, Pedro; Brookhaven National Laboratory, Chemistry Illas, Francesc; Universitat de Barcelona, Departament de Quimica Fisica Rodriguez, Jose; Brookhaven National Laboratory, Chemistry Department

SCHOLARONE™
Manuscripts

Boosting the activity of transition metal carbides towards methane activation by nanostructuring[†]

Marc Figueras,[a] Ramón A. Gutiérrez,[b,c,d] Hèctor Prats,[a] Francesc Viñes,[a] Pedro J. Ramírez,[c,d] Francesc Illas,[a,*] and José A. Rodriguez[b,*]

[a]*Departament de Ciència de Materials i Química Física & Institut de Química Teòrica i Computacional (IQTCUB), Universitat de Barcelona, Martí i Franquès 1-11, 08028 Barcelona, Spain.*
[b]*Chemistry Department, Brookhaven National Laboratory, Upton, New York 11973, United States of America.*
[c]*Facultad de Ciencias, Universidad Central de Venezuela, Caracas 1020-A, Venezuela.*
[d]*Present address: Zoneca-CENEX, R&D Laboratories, Alta Vista, 64770 Monterrey, Mexico*

ABSTRACT

The interaction of methane with pristine surfaces of bulk MoC and Mo_2C is known to be weak. In contrast, a series of X-ray photoelectron spectroscopy (XPS) experiments, combined with thermal desorption mass spectroscopy (TDS), for MoC_y ($y = 0.5 - 1.3$) nanoparticles supported on Au(111)—which is completely inert towards CH_4— show that these systems adsorb and dissociate CH_4 at room temperature and low CH_4 partial pressure. This industrially-relevant finding has been further investigated with accurate density functional theory (DFT) based calculations on a variety of MoC_y supported model systems. The DFT calculations reveal that the MoC_y/Au(111) systems can feature low C-H bond scission energy barriers, smaller than the CH_4 adsorption energy. Our theoretical results for bulk surfaces of Mo_2C and MoC show that a simple Brøensted-Evans-Polanyi (BEP) relationship holds for C−H bond scission on these systems. However, this is not the case for methane activation on the MoC_y nanoparticles as a consequence of their unique electronic and chemical properties. The discovery that supported molybdenum carbide nanoparticles are able to activate methane at room temperature paves the road towards the design of a new family of active carbide catalysts for methane activation and valorisation, with important implications in climate change mitigation and carbon cycle closure.

*Corresponding authors: José A. Rodriguez (rodriguez@bnl.gov), Francesc Illas (francesc.illas@ub.edu)

INTRODUCTION

Natural gas is a common source of energy for heating, cooking, and electricity generation. In this gas, methane (CH_4) is the major component and its activation and transformation can have a major impact in industrial operations and environmental pollution control,[1] given that CH_4 greenhouse capabilities are ~23 times larger than those of carbon dioxide (CO_2),[2] making CH_4 a main role-player of global warming and climate change. Research endeavors have been undertaken to make it possible using CH_4 as a C1 feedstock, an appealing approach for closing the C-cycle[3] while transforming methane into commodity chemicals such as methanol, ethylene, or benzene. However, the high strength of the C-H bonds in CH_4 —4.51 eV·mol^{-1} for the first bond dissociation energy— and the non-polar character of the molecule make the activation of this hydrocarbon particularly difficult. In this respect, it is well known that the methane monooxygenase enzyme is able to activate methane at room temperature. However, this biological system cannot be used in large-scale industrial-scale operations.[4,5] Moreover, to avoid the decomposition of the products and competing reactions, methane activation should proceed at low or medium temperatures.[4,5]These difficulties have triggered a significant amount of research aimed at examining fundamental and practical aspects associated to methane activation by inorganic catalysts, including transition metals, oxides, sulphides, carbides, and zeolites.[5-8]

On late transition metals surfaces, methane binds very weakly and the probability for dissociation is low.[6] For example, on Ni well-defined surfaces, methane dissociation is significant only at temperatures above 450 K;[9] with similar trends reported for Pt and Pd[8] surfaces. Interestingly, low-coordinated surface sites existing in metallic nanoparticles have been found to achieve CH_4 dissociation at or below room temperature even if the ratio of such enhanced activity sites may be too low to lead to large enough conversion.[10,11] In contrast, a few oxide and metal/oxide systems are able to activate methane at 300 K or even lower temperatures.[12,13] On these systems, cooperative interactions between cation and oxide sites are behind the dissociation of the first C-H bond in methane with energy barriers below 0.5 eV.[12,13,14] Transition metal carbides (TMCs) have also been tested as possible catalysts for methane conversion,[7,15-18] although the most stable extended surfaces of typical TMCs such as MoC and TiC exhibit a very low reactivity towards methane with no evidence of dissociation.[7,19] Theoretical calculations suggested that metal-terminated metastable surfaces of carbides could be active for the dissociation of methane.[19,20] However, it is unlikely that such surfaces are exposed when dealing with a bulk TMC under typical reaction conditions although they could well be present in TMC nanoparticles thus representing an interesting possibility. In fact, it is known that TMC nanoparticles supported inside zeolites can catalyse the conversion of methane into ethane,

benzene and other hydrocarbons.[16-18,21] In principle, both the structure of the nanoparticle and its carbon/metal ratio could affect its ability to bind and dissociate methane. However, there is no information regarding this point and no systematic study has been reported so far examining the interaction of methane with TMC nanoparticles.

In this article, we use a combination of experimental and theoretical techniques to investigate the reactivity of MoC_y nanoparticles towards CH_4 activation and dissociation. In particular, we focus on molybdenum carbide (MoC_y) nanoparticles which are growth on an inert Au(111) substrate[22] and employ X-ray photoelectron spectroscopy (XPS), thermal desorption mass spectroscopy (TDS), and density functional theory (DFT) based calculations to examine the interaction of methane with the supported MoC_y nanoparticles. We provide compelling evidence that the MoC_y/Au(111) systems are able to dissociate methane at room temperature. Moreover, for MoC_y nanoparticles with a carbon/metal ratio of 1.1, the CH_x surface groups generated by the adsorption of methane recombine upon heating to yield ethane and ethylene. Our results for bulk surfaces of Mo_2C and MoC show that, following the initial ideas of Pallassana and Neurock,[23] a simple Brøensted-Evans-Polanyi (BEP) relationship[24,25] holds for C−H bond scission on these systems. However, this is not the case for methane activation on the MoC_y nanoparticles as a consequence of their unique electronic and chemical properties.

EXPERIMENTAL DETAILS

The MoC_y/Au(111) systems were prepared following a procedure described in a previous study and established at Brookhaven National Laboratory.[22] On a Au(111) substrate, with the characteristic herringbone $(22×\sqrt{3})$ reconstruction structure, inverse carbide/gold, sulfide/gold and oxide/gold systems have been generated for fundamental studies in catalysis.[22,26-29] In this case, the MoC_y nanoparticles were generated by deposition of Mo metal onto a reactive multilayer of ethylene, which was physisorbed on a Au(111) surface at 100 K. [22] The amount of Mo deposited was estimated using XPS and Mo/Au ratios seen in previous studies for the deposition of Mo on the herringbone structure of Au(111).[22,30,31] The Au(111) substrate does not react with ethylene but the deposited Mo does for form carbide nanoparticles. Upon heating to 750 K, the unreacted ethylene desorbed and MoC_y nanoparticles were left on the gold substrate (Figure S1). This process could be followed using XPS, TDS, and STM.[22] Following this approach, in XPS measurements , we found no O 1s signal and C 1s binding energies which were very different from those of regular hydrocarbons and very close to those reported for molybdenum carbides around 282.5-283 eV (see Figure S1).[32-34] For the Mo 3d core levels, we saw a small shift towards higher binding energy (see Figure S2), consistent with previous

studies for molybdenum carbides and a Mo→C charge transfer.[32,33] In this synthetic process, by changing the initial amounts of Mo and C_2H_4 deposited on the Au(111) substrate, it is possible to control the carbon/molybdenum ratio in the carbide nanoparticles, and this was varied between 0.6 and 1.1. XPS was used to determine this ratio and we utilized as reference previous values measured in our instrument for the C 1s and Mo 3d regions of bulk MoC and Mo_2C.[35] For the bulk sample of MoC, our XPS measurements point to a C/Mo ratio of 0.98-0.96 in good agreement with the ratio typically observed for bulk samples of one-to-one carbides.[29,36-38] A set of the MoC_y/Au(111) surfaces had a C/Mo ratio close to this value but displayed a unique reactivity. Images acquired by scanning tunnelling microscopy (STM) have shown that the MoC_x nanoparticles are small (0.6-1.5 nm) and aggregate in the face-centred cubic (fcc) troughs located on either side of the elbows of the reconstructed Au(111) surface.[22] Previous and current images of STM indicate that the nanoparticles are essentially amorphous and do not have the typical structures of bulk MoC or Mo_2C.[22] Thus, due to their size and structure, these nanoparticles can have special chemical and catalytic properties.

The reactivity of the MoC_y/Au(111) surfaces towards methane was examined in a system which combines an ultrahigh-vacuum (UHV) chamber (base pressure $\sim 7 \cdot 10^{-10}$ mbar) and a batch reactor.[39-42] Within this system, the sample could be transferred between the reactor and UHV chamber without exposure to air. The UHV chamber was equipped with instrumentation for XPS, ultraviolet photoelectron spectroscopy (UPS), low-energy electron diffraction (LEED), ion scattering spectroscopy (ISS), and TDS. In the tests to study the interactions with methane, clean Au(111) and MoC_y/Au(111) surfaces were positioned in the batch reactor at $\sim$ 300 K, then 1 Torr of CH_4 was introduced for a period of five minutes. After this exposure, the CH_4 gas was removed and each sample was transferred back to the UHV chamber for surface characterization with XPS and TDS.

COMPUTATIONAL METHODS AND MODELS

Methane activation on MoC_y/Au(111) has been assessed by modelling different Au-supported MoC_y nanoparticles with C/Mo ratios ranging from 0.67 to 1.50, as in the experiments, and relying on periodic DFT based calculations. The initial stoichiometric structures of MoC nanoparticles in gas-phase were taken so as to mimic the most stable gas-phase TiC nanoparticles reported in previous work by Lamiel *et al.*, [43] formerly obtained by data mining searches combining interatomic potentials and DFT calculations. These authors reported a total of nine Ti_6C_6 and twelve $Ti_{12}C_{12}$ low energy structures. In the present work, these structures were taken as initial guess for the gas-phase Mo_6C_6 and $Mo_{12}C_{12}$ nanoparticles by simply replacing all Ti atoms by Mo atoms followed by full PBE-D3 relaxation without any constraint. Interestingly, for both sizes, the structure of the most stable MoC isomer corresponds to the most stable one for the TiC nanoparticle. However, in some cases, the order

of stability of the other (*i.e.*, less stable in gas-phase) MoC isomers differs from that of their TiC counterparts. To obtain suitable non-stoichiometric structures in gas-phase, mimicking the composition of the particles in the experiments, a cascade approach was used starting from the two most stable Mo_6C_6 and $Mo_{12}C_{12}$ structures. The different non-stoichiometric nanoparticles were created removing one of all non-equivalent (Mo or C) atoms at a time. This resulted in five Mo_5C_6, four Mo_6C_5, six $Mo_{11}C_{12}$, and other six $Mo_{12}C_{11}$ new structures with C/Mo ratios between 0.83 to 1.20. To fill the experimental ratio ranging from 0.6 to 1.1, structures resulting from successive extractions of one Mo or one C atom were considered as well. Overall, a full set of 148 gas-phase non-stoichiometric MoC_y structures were obtained and their structure fully optimized.

The two most stable Mo_6C_6 (Mo_6C_6-1 and Mo_6C_6-2) and the most stable $Mo_{12}C_{12}$ structures in gas-phase were supported on the Au(111) surface. This step implied a large number of geometry optimizations due to the high number of possible orientations of the supported nanocluster and the presence of different adsorption sites on the Au(111) surface. All MoC_y/Au(111) systems were optimized, and the structure presenting the strongest adsorption energy was chosen to perform the study of CH_4 adsorption and dissociation, the latter making use of the climbing-image nudged elastic band (CI-NEB) algorithm. Similarly, the most stable non-stoichiometric Mo_6C_5, Mo_6C_4, Mo_4C_6, $Mo_{12}C_{10}$, and $Mo_{10}C_{12}$ structures in gas-phase were supported on Au(111). Again, for each non-stoichiometric structure, the optimized geometry presenting the strongest adsorption energy was chosen to perform the study of CH_4 adsorption and dissociation. In summary, three stoichiometric —two isomers of Mo_6C_6 and one of $Mo_{12}C_{12}$— and five non-stoichiometric nanoparticles supported on Au(111) were investigated, as shown in Figure 1. These carbide nanoparticles have diameters which are within the range of sizes experimentally found with STM for MoCy/Au(111) systems.[22] For comparison, the extended C- and Mo-terminated orthorhombic β-Mo_2C(0001) and cubic δ-MoC(001) surfaces have been studied as well.

All present DFT calculations employed the Perdew-Burke-Ernzerhof (PBE)[44] exchange-correlation (xc) functional, known to accurately describe molybdenum carbide and transition metal surfaces.[45,46] The dispersion —van der Waals, vdW— term was approximated through the D3 correction as proposed by Grimme.[47] Spin polarization was taken explicitly into account only for the systems containing non-stoichiometric MoC_y nanoparticles in gas phase as test calculations show that any spin polarization is quenched once the particles are supported on the Au(111) metallic surface. The transition state (TS) structures for methane dissociation were located using the climbing-image nudged-elastic-band (CI-NEB) method[48] employing five intermediate images, and the gained TS further characterized by appropriate frequency analysis. Initial guesses for those images were

generated by means of the atomic simulation environment (ASE)[49] using the image dependent pair potential (IDPP).[50] All calculations were carried out using the Vienna *ab Initio* simulation package (VASP).[51] Further computational details and obtained geometries are provided in the ESI. Note in passing by that favourable adsorption energies, E_{ads}, are defined negative, and all reported energy values include the zero-point energy (ZPE) term obtained within the harmonic approximation.

RESULTS AND DISCUSSION

Experiments. Figure 2 shows a C 1*s* XPS spectrum obtained after exposing clean Au(111) to 1 Torr of methane at 300 K. The noble metal did not react with methane at room or elevated temperatures. This agrees with previous studies which show that this substrate also does not react with ethylene.[22] At low and high temperatures pure metallic gold is not able to break the C-H bonds in the hydrocarbon, even in presence of adsorbed atomic O.[52] Included in Figure 2 is a C 1*s* spectrum collected after exposing bulk polycrystalline δ-MoC to 1 Torr of CH_4 at 300 K. Only features for the carbon atoms in the carbide are observed. In the region between 284 and 285 eV, where signal for CH_x fragments is usually seen, [7] no clear features are detected and one sees the plain C 1*s* spectrum of a metal carbide. From previous studies it is known that samples of bulk polycrystalline δ-MoC or TiC do not react with methane at room temperature.[7,19] The surface metal atoms of such bulk 1:1 TMCs are saturated with C atoms, and so do not attack the C-H bonds in methane,[7,19]

Thus, the blank experiments in Figure 2 show that neither Au(111) nor bulk δ-MoC is useful for methane activation. In contrast, we found a different behaviour for MoC_y ($y = 0.6 - 1.1$) nanoparticles dispersed on Au(111). These nanoparticles do react with methane at room temperature, and the strength of the interaction appears to be affected by the carbon/metal ratio of the studied system. Figure 3 displays C 1*s* XPS spectra collected after dosing methane at 300 K to a Au(111) surface pre-covered with 0.3 monolayers (ML) of $MoC_{0.6}$. The fresh sample shows the typical C 1*s* XPS peak position at ~283 eV, expected for a molybdenum carbide.[22] Upon exposure to methane a second peak appears *circa* 284.8 eV, which cannot be attributed to adsorbed CH_4 and indicates the generation of CH_x (x= 1,2,3) species on top of the carbide surface.[7,13,14] This peak has a full width at half maximum (FWHM) of ~ 1.5 eV, very similar to that measured for bulk MoC and the carbide nanoparticles dispersed on gold. Annealing to 500 and 600 K induces the disappearance of the CH_x features while the features for MoC_y grow. Figure 4 shows the relative changes in the CH_x and MoC_y signals as a function of temperature, and from it one deduces that the $MoC_{0.6}$/Au(111) seems to be metastable in the presence of CH_4, and while the Mo attacks the C atoms in CH_x the carbon/metal ratio in the carbide appears to increase. A similar behaviour has been seen for bulk Mo_2C in an atmosphere of methane or other hydrocarbons at high temperatures where a $Mo_2C \rightarrow MoC$ transformation was seen

6

with *in-situ* X-ray diffraction for powders of the carbide.[53] When compared to bulk Mo_2C, our results indicate that the $MoC_{0.6}$ nanoparticles are more chemically active, as they do react with CH_4 at room temperature, although their low stability gives them a limited use as catalysts.

In bulk carbides of molybdenum, an increase in the carbon/metal ratio from 0.5 to 1 leads to a MoC compound which has a negligible reactivity towards methane, as seen in Figure 2 and in previous studies.[7,19] In the case of the MoC_y nanoparticles, the reactivity towards CH_4 is also affected by the C/Mo ratio, but for these nanostructures, at ratios higher than one, there is still significant reactivity towards methane. Figure 5 shows the C 1*s* XPS spectra recorded after dosing methane at 300 K to a Au(111) surface pre-covered with 0.3 ML of $MoC_{1.1}$. The fresh sample shows again the typical C 1*s* features for a carbide near ~283 eV,[22] and the dosing of methane leads to the appearance as well of a second peak near 284.5 eV due to adsorbed CH_x. Thus, when going from C-meagre to C-rich nanoparticles —$MoC_{0.6}$ to $MoC_{1.1}$— the system is still able to dissociate methane at room temperature, although the adsorbed CH_x binding weakens, since, as shown in Figures 5 and 6, a minor temperature increase triggers a rapid decrease in the CH_x signal intensity without, however, significantly affecting the C 1s signal intensity assigned to the MoC_y carbide. Therefore, the $MoC_{1.1}$ nanoparticles appear to be stable under an atmosphere of methane. This behaviour is reminiscent of that observed for MoC powders [30] and bulk crystals of 1:1 TMCs.[5] Indeed, we found that the $MoC_{1.1}$/Au(111) system was able to sustain many CH_4 adsorption/desorption cycles without any significant change neither on the C/Mo ratio nor in the reactivity of the surface towards CH_4 (Figure 7). Thus, in the $MoC_{1.1}$ nanoparticles, one has the right balance of stability and activity making them useful as catalysts.

As far as the chemical behaviour of adsorbed CH_x is concerned, mass spectrometer signals detected mainly the evolution of CH_4 from the CH_x/$MoC_{1.1}$/Au(111) surface, as a consequence of a $CH_{x,ads} + (4-x)\cdot H_{ads} \rightarrow CH_{4,gas}$ recombination, but with noticeable signals for C_2H_6 and C_2H_4, see Figure 8. No CO or water desorption was found, consistent with a lack of an O 1s XPS signal after preparing the carbide overlayer or after dosing methane. In average, the relative amount of the desorbed hydrocarbons from the CH_x/$MoC_{1.1}$/Au(111) surface was methane (79%), ethane (15%), and ethylene (7%). Thus, it is clear that the species produced by the CH_4 dissociation are chemically active and so susceptible to be used for producing other, more complex hydrocarbons. Indeed, one can envision that nanoparticles of the $MoC_{1.1}$ type could be responsible for the activity seen over MoC_x/ZSM-5 catalysts when transforming methane into larger hydrocarbons.[16-18,21]

Computational study. To disclose the chemistry behind the described experiments for the MoC_x/Au(111) systems, methane adsorption and first C-H bond scission have been studied on eight different supported MoC_y nanoparticles with C/Mo ratios ranging from 0.67 to 1.50, as in the

experiments. For comparison, similar calculations have been carried for the extended C- and Mo-terminated β-Mo$_2$C(0001) and δ-MoC(001) surfaces. The interaction of all the above stated nanoparticles with the Au(111) surface has been studied by explicitly and systematically placing the MoC$_y$ center of mass above several non-equivalent sites (*i.e.*, top, bridge, and hollow sites) and exploring several orientations per site as described in the section on Computational Methods and Models. A similar procedure has been used to explore the structure of CH$_4$, CH$_3$, and H moieties when adsorbed on the supported clusters, where η^1, η^2, and η^3 connectivities have been considered for CH$_4$.[19]

The present calculations show that, in general, CH$_4$ prefers to adsorb on low-coordinated Mo atoms with η^2 connectivity, see Figure 9, featuring surprisingly high adsorption energies, ranging from -0.38 to -1.16 eV, see PBE-D3 E_{ads} values listed in Table 1, thus suggesting a clear meeting point in between the Mo special affinity towards CH$_4$ and the low-coordination effect.[10,19] Clearly, the MoC$_y$ nanoparticles exhibit E_{ads} values larger than the extended surface, which range from -0.17 to -0.39 eV only —see the optimized geometries in Figure 10. Similarly, CH$_3$ species also prefer low-coordinated Mo atoms, which agrees with the experimental finding that C-poor MoC$_y$ nanoparticles present a stronger binding towards CH$_x$ species. Finally, atomic H can be adsorbed indistinguishably at both top-C or top-Mo sites. Note also that, since the removing one carbon atom does not produce a significant structural reconstruction, the most stable Mo$_6$C$_6$ isomer (Mo$_6$C$_6$-1) and Mo$_6$C$_5$ structures are actually very similar, see Figure 1. The CH$_4$ adsorption and subsequent dissociation in the latter structure has been studied by considering the most stable adsorption site near the C vacancy defect. The same strategy has been used on the Mo$_{10}$C$_{12}$ structure, since it is very similar to Mo$_{12}$C$_{12}$, except near the Mo vacancy defect.

For the eight selected supported MoC$_y$ structures, as well as for the above mentioned extended δ-MoC and β-Mo$_2$C surfaces, we have carried out TS searches for CH$_4$ dissociation by using the CI-NEB method. Specifically, the dissociation of an adsorbed CH$_4$ molecule from its most stable adsorption site to produce CH$_3$, typically remaining in the same site, and one atomic H typically ended adsorbed in the most stable nearby site, has been studied. Note that, for every structure, several dissociation energy paths —between 3 to 7 depending on the chosen structure— have been explored with different final configurations, so as to have a clear, unequivocal description of the CH$_4$ dissociation energy landscape. The optimized geometries for all obtained TSs are reported in Figures S3 and S4 of the ESI. The energy barriers values, reported in Table 1, are thus the lowest among the explored energy paths. Regarding the C-terminated β-Mo$_2$C(0001) and δ-MoC (001) extended surfaces, the CH$_4$ adsorption energy is always much smaller than the energy barrier for dissociation, in agreement with experimental findings that these surfaces do not dissociate methane, and implying

a preference for desorption rather than for dissociation. In the case of the Mo-terminated β-$Mo_2C(0001)$ surface, the energy barrier is *circa* 0.1 eV larger that the adsorption energy, indicating that this particular surface may exhibit some activity towards methane, also in agreement with experiments. However, most of the studied $MoC_y/Au(111)$ systems feature energy barriers for dissociation equal or lower than the adsorption energy of methane, with the only exceptions of Mo_4C_6 and $Mo_{10}C_{12}$, suggesting that MoC_y nanoparticles with $y > 1.2$ present a lower activity compared to other nanoparticles.

The analysis of DFT results also permits to identify the nanocluster size effect on the CH_4 dissociation energy barrier, *i.e.* by comparing results for most stable Mo_6C_6 and $Mo_{12}C_{12}$ structures. For both supported clusters, the energy barriers for CH_4 dissociation are quite similar, 0.58 and 0.60 eV, respectively. Consequently, the effect of nanoparticle size may not be significant, at least for stoichiometric structures, although, obviously, this preliminary statement would be confirmed when data for larger nanoparticles could be acquired. Nevertheless, the present results indicate that the effect of the nanocluster shape seems to play a dominant role. Take, for instance, the supported Mo_6C_6 nanoparticles, where the methane dissociation energy barriers for the most stable (Mo_6C_6-1) and second most stable (Mo_6C_6-2) supported structures are 0.58 and 1.02 eV, respectively. Clearly, the large difference in the calculated energy barriers is to be attributed to the large structural difference which is clearly seen in Figure 1. Finally, the results reported in Table 1 suggest that the C-H scission energy barrier on Mo-deficient systems is very similar to their stoichiometric homologs. The case of C-meagre systems is especially interesting since feature much lower energy barriers which may be as low as 0.08 eV for Mo_6C_4, an exceptional result that perfectly agrees with the experimental observation that $MoC_{0.6}$ nanoparticles are the most reactive ones.

Unravelling trends for C-H bond activation on bulk surfaces and nanostructures of molybdenum carbides. To further investigate key points in the activation of the C-H bond in CH_4 on different systems of molybdenum carbide we investigated trends for the adsorption and dissociation of the hydrocarbon on the bulk surfaces and nanostructures examined. In a past study a clear correlation was found when comparing E_b for CH_4 dissociation *vs.* E_{reac} (*i.e.*, BEP relationship) on Ni/TiC(001) systems and on bare Ni(111). [7] Figure 11 shows that this type of correlation holds well comparing the results for the adsorption and dissociation of methane on the bulk surfaces of δ-MoC and β-Mo_2C (the latter with two possible terminations). However, for the nanoparticles there are deviations of the linearity which are a strong indication of a different underlying chemistry. The results in Figure 11 indicate that the reactivity of the finite nanoparticles cannot be extrapolated from the behavior seen for the extended bulk carbides. In general, the breakdown of the correlation is mainly a consequence of a lowering in the energy barrier for the $CH_4 \rightarrow CH_3+H$ dissociation on the carbide nanoparticles, while

keeping similar reaction energies to those for extended carbides. As discussed above, this lowering is a consequence of the existence of special low-coordinated Mo atoms in the vertices of the nanostructures. The energy barriers for methane dissociation on the most active MoC_y nanoparticles are close to those calculated on $IrO_2(110)$ and $Ni/CeO_2(111)$ surfaces.[12,13] On those systems, a concerted mechanism has been reported for low-temperature activation where the cleavage of the first C−H bond in methane involves simultaneous bonding interactions with a metal cation and an oxygen anion.[12,13] This type of dissociative interaction cannot take place on the MoC_y nanoparticles where the C centers do not have the very high negative charge present in the O centers of an oxide. Nevertheless, the η^2 connectivity on Mo atoms seen in Figure 9 is very efficient for the activation of methane. Such a type of dissociative interaction probably occurs when nanoparticles of MoC_y are dispersed in the cages of zeolites and methane is transformed into ethane, benzene and other hydrocarbons.[16-18,21]

CONCLUSIONS

The present experimental and theoretical results point to a clear enhancement in the reactivity of the MoC based systems towards methane activation when going from extended surfaces to the case of MoC_y ($y = 0.5 - 1.3$) nanoparticles supported on Au(111). The supported MoC_y nanoparticles are able to dissociate CH_4 at room temperature, and the activity, the stability, and the strength of the interaction with CH_x species appears to depend on the C/Mo ratio. While C- deficient nanoparticles are very reactive, they feature low stability due to the strong binding of the adsorbed CH_x species, which leads to an increase in the C/Mo ratio upon annealing. On the other hand, Mo-deficient systems present the right balance of stability and activity. Although, Mo-deficient nanoparticles are less reactive, they are still able to dissociate methane at room temperature, and are stable under an atmosphere of methane, posing themselves as attractive catalytic systems towards CH_4 capture and catalytic conversion.

The present exciting and technologically relevant experimental result were explained by means of DFT based calculations on a broad enough set of supported MoC_y nanoparticles models with C/Mo ratios ranging from 0.67 to 1.50. The DFT calculations confirm that supported carbide nanoparticles feature stronger CH_4 adsorption energies than extended δ-MoC or β-Mo_2C surfaces, with adsorption energy values up to -1.16 eV. Moreover, the energy barrier for CH_4 dissociation on the nanoparticles gets substantially reduced, and can be as low as 0.08 eV for C-deficient systems, perfectly agreeing with the experimental findings. All in all, the present results open the way for the preparation of a new family of active catalysts for methane activation and conversion under mild conditions, thus widening the applications of existing natural gas resources.

CONFLICTS OF INTEREST

The authors declare no conflict of interest.

ACKNOWLEDGEMENTS

Figure 1. Optimized geometries (top and side views) for the studied $MoC_y/Au(111)$ systems. Au, Mo, C, and H atoms are shown as yellow, blue, black, and white spheres, respectively. In all cases, the most stable isomer has been studied, except for the Mo_6C_6, where the second most table structure was also studied (Mo_6C_6-2).
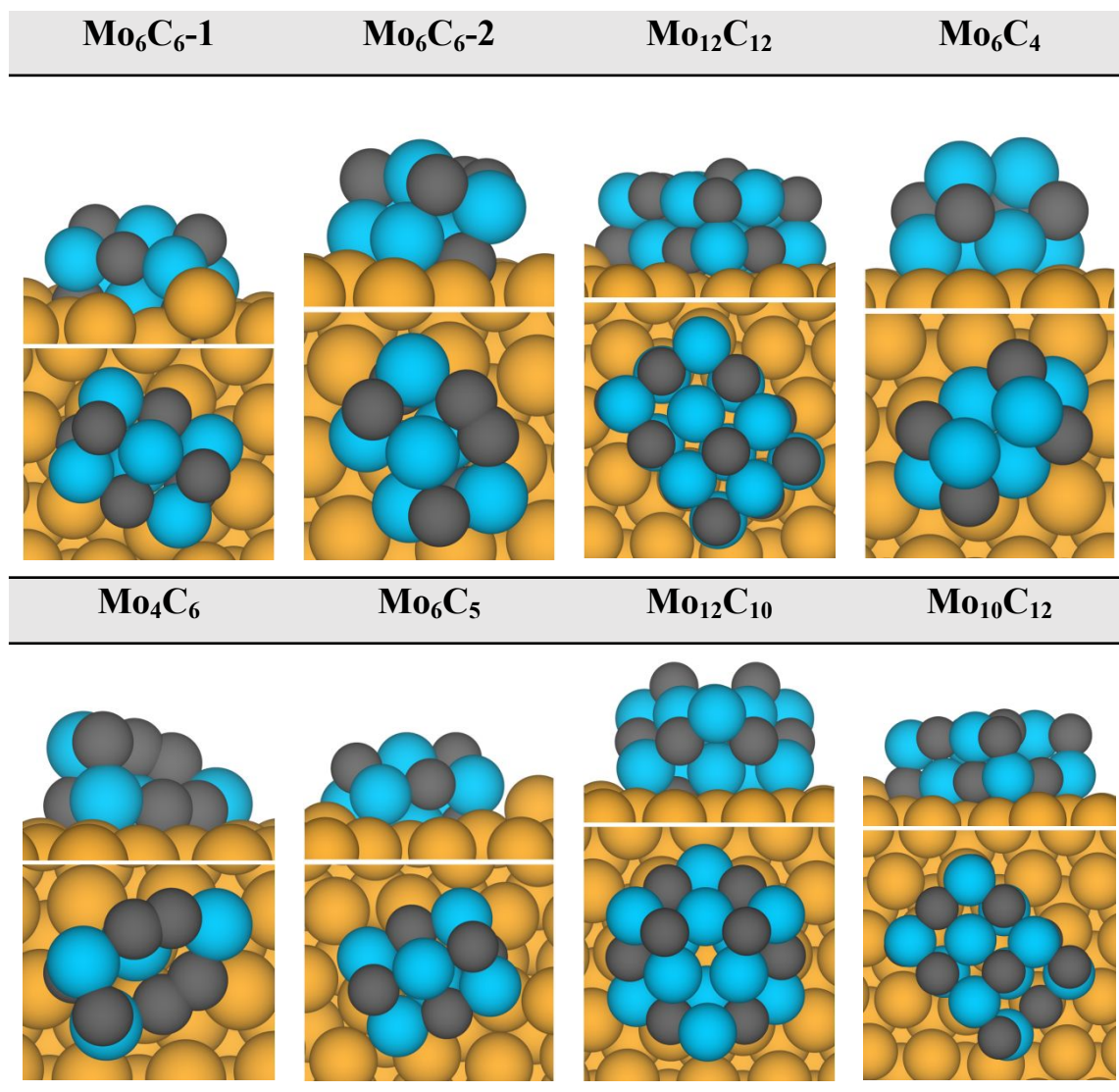
Figure 2. C 1*s* XPS spectra collected after dosing methane to clean Au(111) and bulk polycrystalline δ-MoC. The dosage of methane was 1 Torr for 5 minutes.
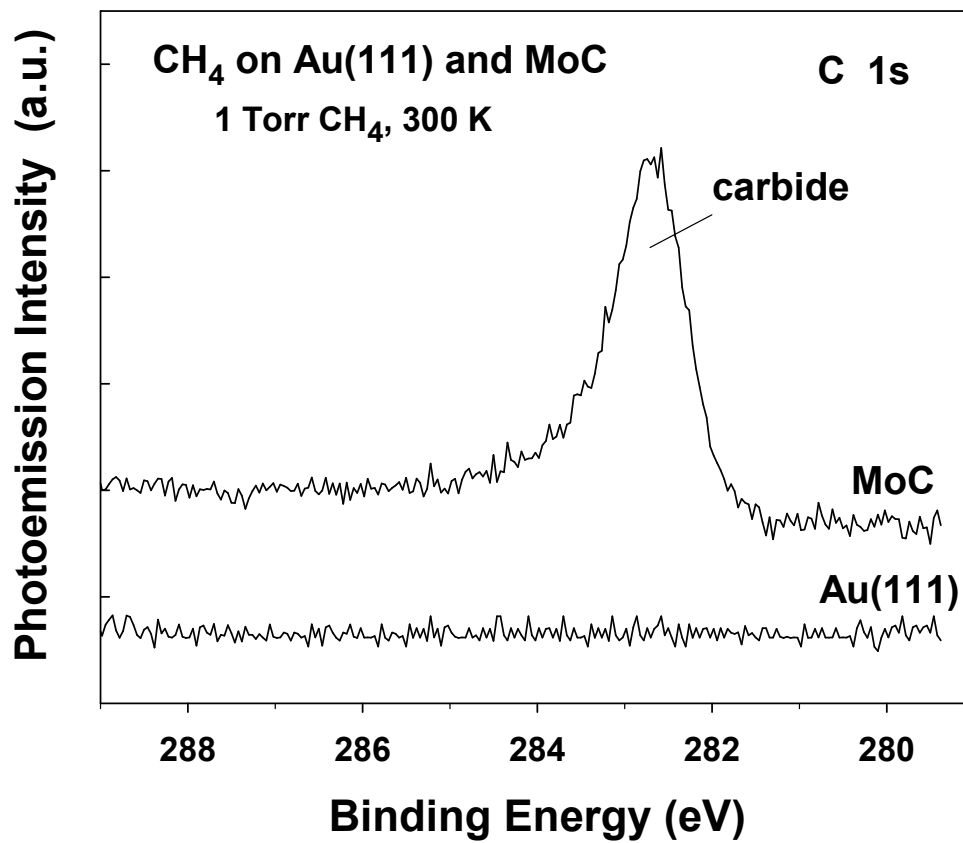
Figure 3. C 1*s* XPS spectra collected before and after dosing methane to $MoC_{0.6}$/Au(111) at 300 K. This was followed by heating to 400, 500, and 600 K. The dosage of methane was 1 Torr for 5 minutes. The initial coverage of $MoC_{0.6}$ on the Au(111) substrate was 0.3 ML.
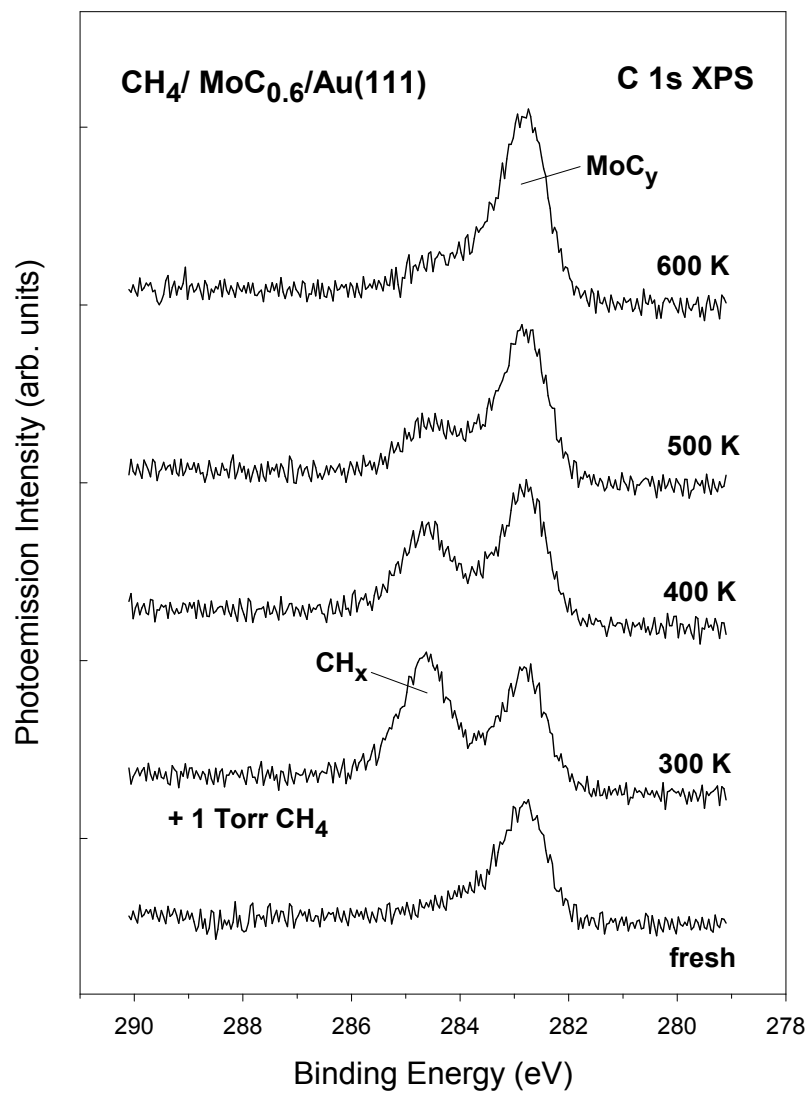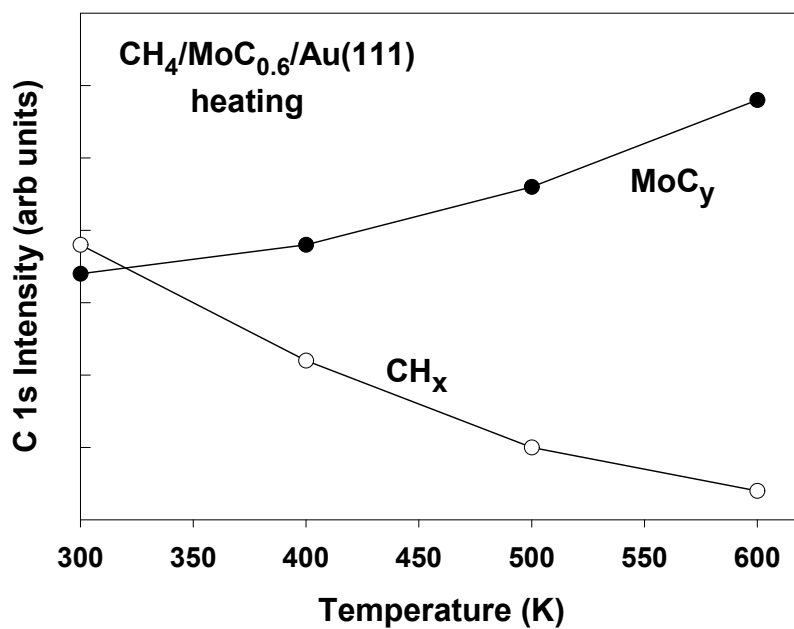
Figure 4. Variation of the CH$_x$ and MoC$_y$ intensities as a function of temperature in CH$_4$/MoC$_{0.6}$/Au(111). Initially the surface was exposed to 1 Torr of methane for 5 minutes at 300 K, see Figure 1.

Figure 5. C 1s XPS spectra collected before and after dosing methane to MoC$_{1.1}$/Au(111) at 300 K. This was followed by heating to 350, 400, 450, and 500 K. The dosage of methane was 1 Torr for 5 minutes. The initial coverage of MoC$_{1.1}$ on the Au(111) substrate was 0.3 ML.
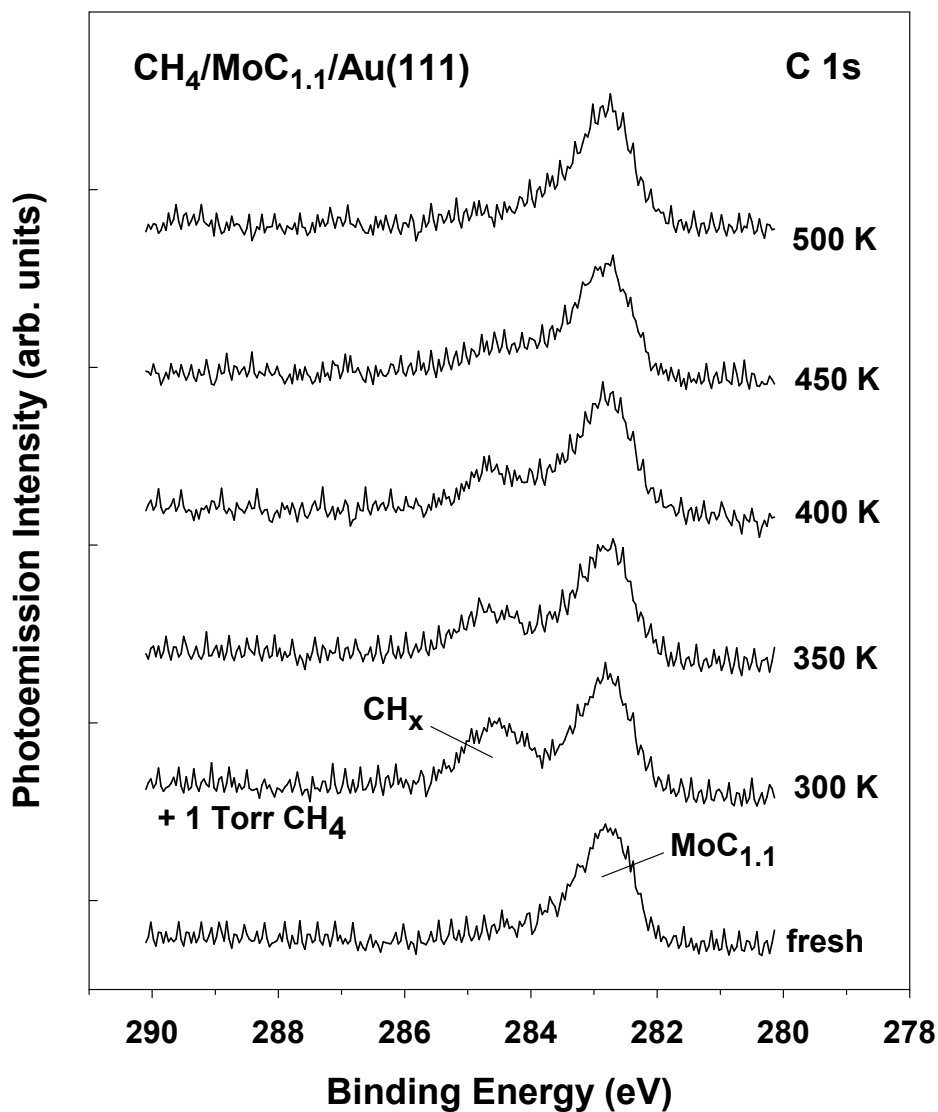
Figure 6. Variation of the CH_x and MoC_y intensities as a function of temperature in $CH_4/MoC_{1.1}/Au(111)$. Initially the surface was exposed to 1 Torr of methane for 5 minutes at 300 K, see Figure 3.
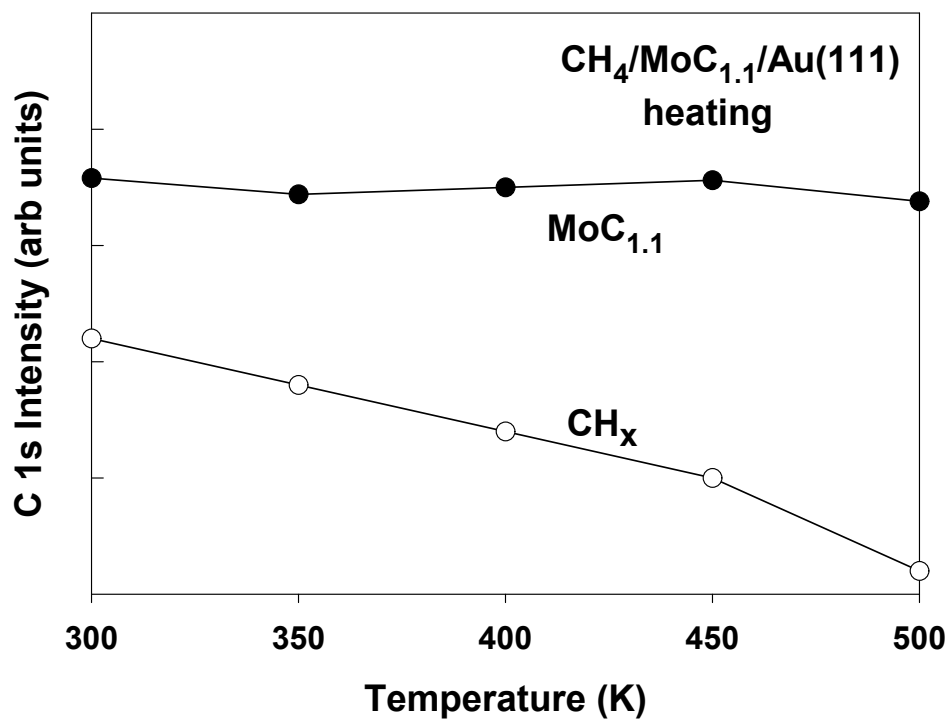
Figure 7. Top panel: C 1*s* XPS spectra collected after 1 and 5 cycles of adsorption/desorption for the $CH_4/MoC_{1.1}/Au(111)$ at 300 K. In each cycle, the surface was exposed to 1 Torr of CH_4 at 300 K for five minutes. Then, the gas was removed, the corresponding C 1*s* XPS spectrum was recorded, and finally the sample was heated to 500 K to desorb the CH_x deposited before the beginning of the next cycle. This was repeated for five cycles. Bottom: Amount of CH_x adsorbed in each cycle after dosing methane at 300 K. The initial coverage of $MoC_{1.1}$ on the Au(111) substrate was 0.3 ML and essentially remained constant after five cycles.
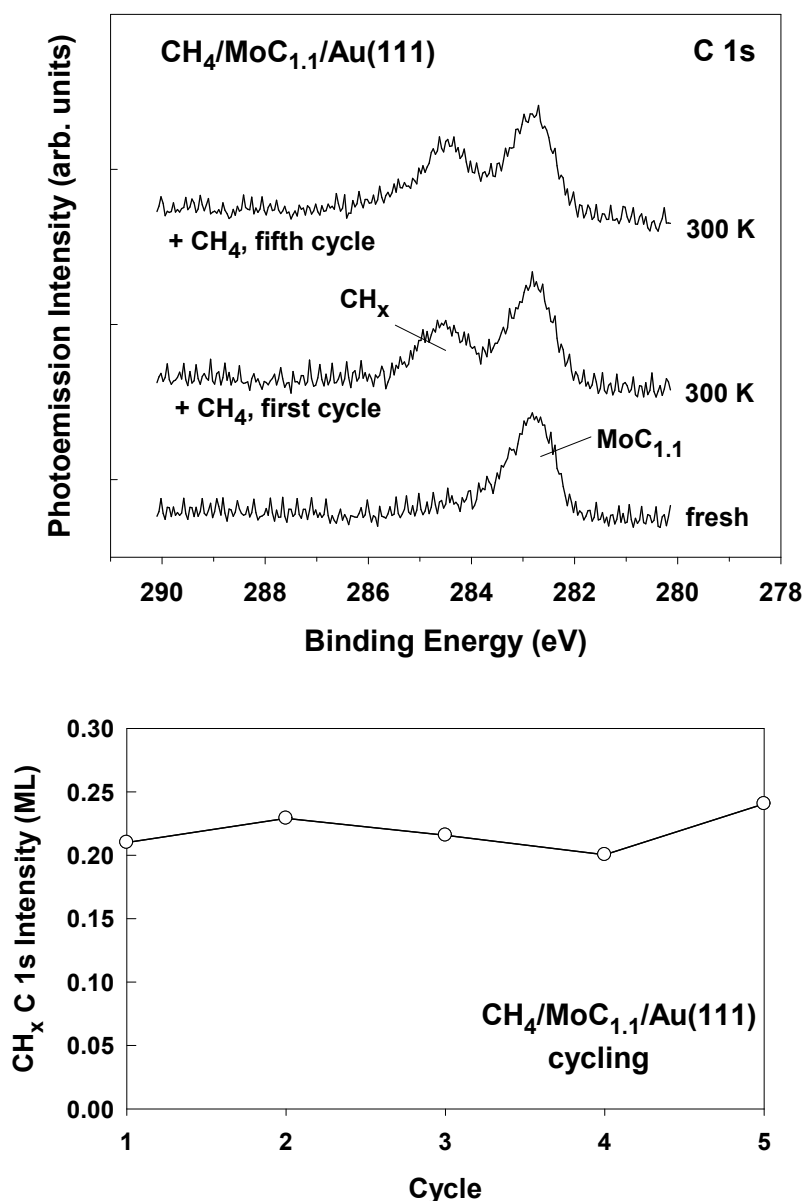
Figure 8. Thermal desorption spectra collected after exposing a $MoC_{1.1}/Au(111)$ surface to 1 Torr of methane for 5 minutes at 300 K in a micro-reactor. The gas was pumped out and the sample was transferred to a UHV chamber for a TDS study (heating ramp 2 K/s).
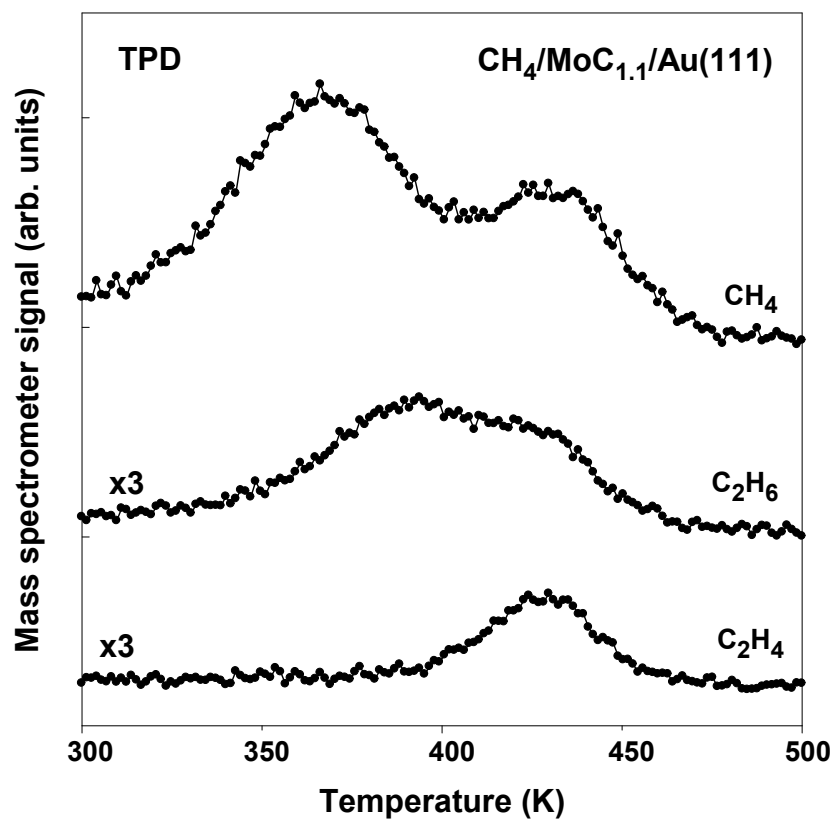
Figure 9. Optimized geometries (top and side views) for the adsorption of CH_4 on all studied $MoC_y/Au(111)$ systems. Au, Mo, C, and H atoms are shown as yellow, blue, black, and white spheres, respectively. In all cases, the most stable isomer has been studied, except for the Mo_6C_6, where the second most table structure was also studied (Mo_6C_6-2).
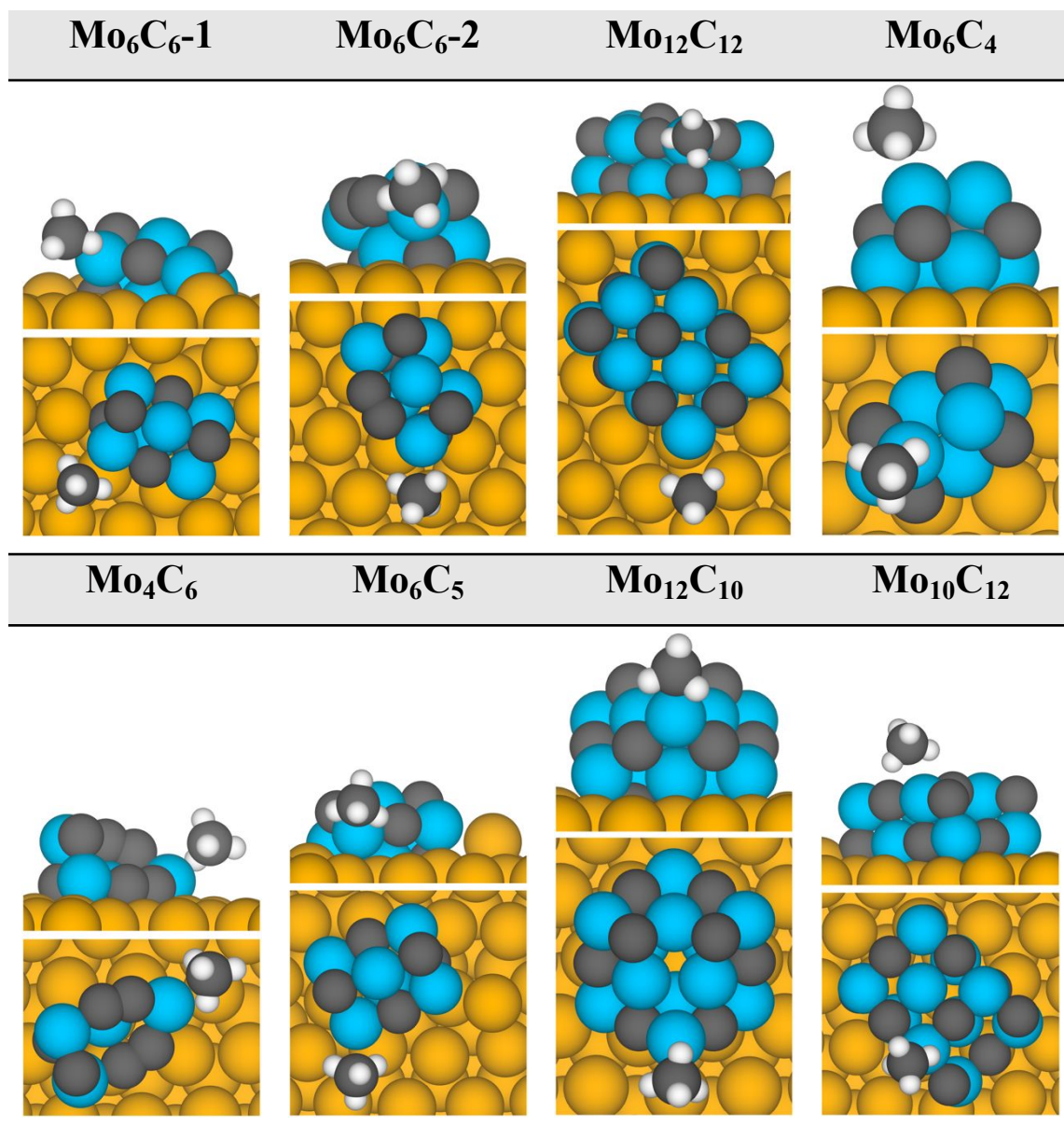
Figure 10. Optimized geometries (top and side views) for the adsorption of methane on δ-MoC(001) and C/Mo-terminated β–Mo$_2$C(0001) surfaces. Colour code as in Figure S1.
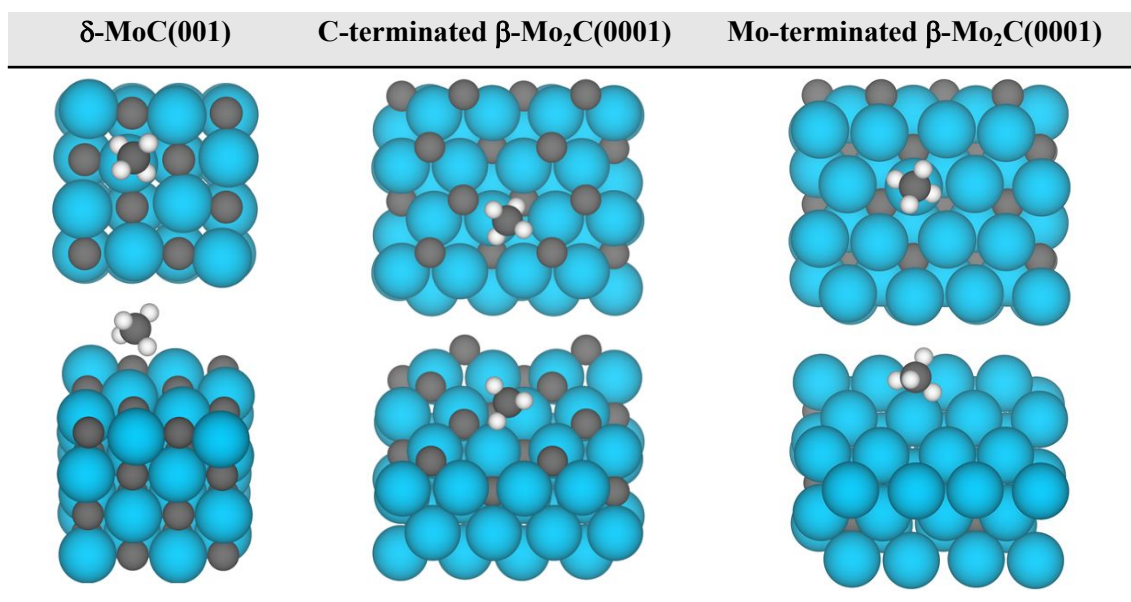

δ-MoC(001)	C-terminated β-Mo$_2$C(0001)	Mo-terminated β-Mo$_2$C(0001)

Table 1. Methane adsorption energies *(E_ads)* and energy barriers (E_b) and reaction energies (E_{reac}) for CH$_4$ dissociation on all studied systems.

System	E_{ads} (eV)	E_b (eV)	E_{reac} (eV)
Mo$_6$C$_6$-1	-1.16	0.58	-0.68
Mo$_6$C$_6$-2	-0.95	1.02	-0.79
Mo$_{12}$C$_{12}$	-0.61	0.60	-0.33
Mo$_6$C$_4$	-0.48	0.08	-1.98
Mo$_4$C$_6$	-0.38	0.63	-1.03
Mo$_6$C$_5$	-0.45	0.58	-0.55
Mo$_{12}$C$_{10}$	-0.51	0.37	-0.62
Mo$_{10}$C$_{12}$	-0.22	0.58	-1.57
δ-MoC(001)	-0.17	1.20	0.59
C-terminated β-Mo$_2$C(0001)	-0.18	0.67	-0.66
Mo-terminated β-Mo$_2$C(0001)	-0.39	0.48	-1.66

Figure 11. Energy barrier (E_b) for CH_4 to CH_3+H dissociation on different molybdenum carbide nanoparticles (black triangles) and extended surfaces (blue dots) versus the reaction energy (E_{reac}). The values used to construct the plot are reported in Table 1. The linear regression corresponds to the values from the extended surfaces only.
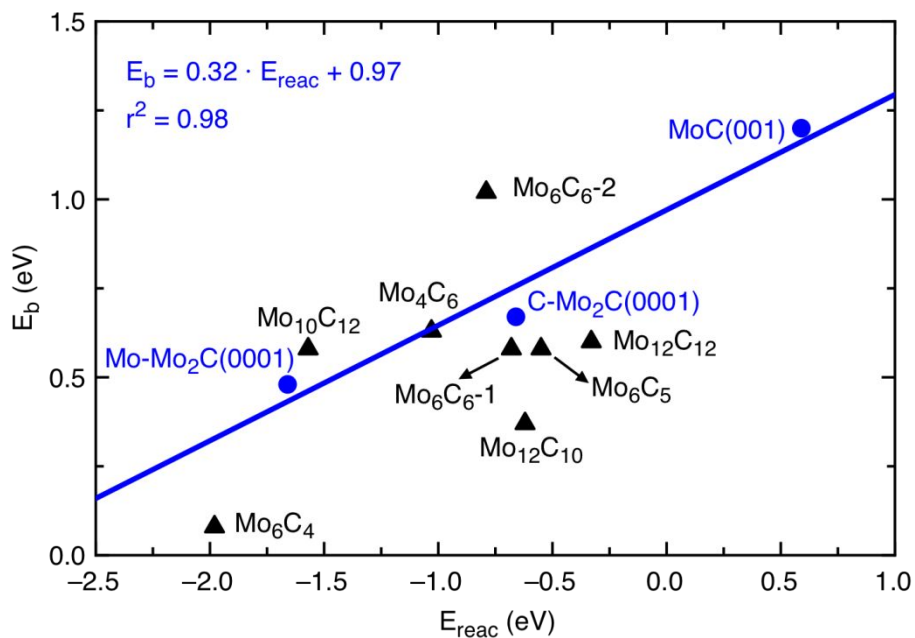
NOTES AND REFERENCES

[1] P. Tang, Q. Zhu, Z. Wu and D. Ma, *Energy Environ. Sci.,* 2014, **7**, 2580–2591.

[2] J. Feichter, U. Schurath and R. Zellner, *Chem. Unserer Zeit,* 2007, **41**, 138-150.

[3] D. L. Woodard, S. J. Davis and J. T. Randerson, *Proc. Natl. Acad. Sci.,* 2019, **116**, 759-764.

[4] S. I. Chan and S. S. Yu, *Acc. Chem. Res.,* 2008, **41**, 969–979.

[5] M. Ravi, V. L. Sushkevich, A. J. Knorpp, M. A. Newton, D. Palagin, A. B. Pinar, M. Ranocchiari and J. A. van Bokhoven, *Nature Catal.* 2019, **2**, 485–494.

[6] P. Khirsariya and R. K. Mewada, *Procedia Engineering,* 2013, **51**, 409–415.

[7] H. Prats, R. A. Gutiérrez, J. J. Piñero, F. Viñes, S. T. Bromley, P. J. Ramírez, J. A. Rodriguez and F. Illas, *J. Am. Chem. Soc.,* 2019**, 141**, 5303-5313.

[8] T. V. Choudhary, E. Aksoylu and D. W. Goodman, *Catal. Rev.,* 2003, **45**, 151–203.

[9] T. P. Jr. Beebe, D. W. Goodman and B. D. Kay, *J. Chem. Phys.,* 1987, **87**, 2305-2315.

[10] F. Viñes, Y. Lykhach, T. Staudt, C. Papp, H.-P. Steinrück, J, Libuda, K. M. Neyman and A. Görling, *Chem. Eur. J.,* 2010, **16**, 6530-6539.

[11] S. M. Kozlov and K. M. Neyman, *J. Catal.,* 2017, **336**, 111-121.

[12] Z. Liang, T. Li, M. Kim, A. Asthagiri and J. F. Weaver, Surface. *Science,* 2017, **356**, 299–303.

[13] Z. Liu, D. G. Grinter, P. G. Lustemberg, T.-D. Nguyen-Phan, Y. Zhou, S. Luo, I. Waluyo, E. J. Crumlin, D. J. Stacchiola, J. Zhou, J. Carrasco, H. F. Busnengo, M. V. Ganduglia-Pirovano, S. D. Senanayake and J. A. Rodriguez, *Angew. Chem. Int. Ed.,* 2016, **55**, 7455–7459.

[14] P. G. Lustemberg, P. J. Ramírez, Z. Liu, R. A. Gutiérrez, D. G. Grinter, J. Carrasco, S. D. Senanayake, J. A. Rodriguez and M. V. Ganduglia-Pirovano, *ACS Catal.,* 2016, **6**, 8184−8191.

[15] H. F. Li, Z.-Y. Li, Q.-Y. Liu, X.-N. Li, Y.-X. Zhao and S.-G. He, *J. Phys. Chem. Lett.,* 2015, **6**, 2287-2291.

[16] F. Solymosi, A. Szöke and J. Cserény, *Catal. Lett.,* 1996, **39**, 157–161.

[17] N. K. Razdan, A. Kumar and A. Bhan, *J. Catal.,* 2019, **372**, 370-381.

[18] M. Rahman, A. Sridhar and S. J. Khatib, *Applied Catal. A: General,* 2018, **558**, 67-80.

[19] S. Posada-Perez, J. R. dos Santos Politi, F. Viñes and F. Illas, *RSC Advances*, 2015, **5**, 33737-33746.

[20] T. Zhang, X. Yang and Q. Ge, *Catal. Today,* 2019, DOI: 10.1016/j.cattod.2019.03.020

[21] W. Ding, S. Li, G. D. Meitner and E. Iglesia, *J. Phys. Chem. B,* 2001, **105**, 506-513.

[22] J. M. Horn, Z. Song, D. V. Potapenko, J. Hrbek and M. G. White, *J. Phys. Chem. B,* 2005, **109**, 44-47.

[23] V. Pallassana and M. Neurock, *J. Catal*., 2000, **191**, 301-317.

[24] J. N. Brønsted, *Chem. Rev*. 1928, **5**, 231-338.

25 M. G. Evans and M. Polanyi, *Trans. Faraday Soc*., 1938, **34**, 11-24.

26 T. Cai, Z. Song, J. A. Rodriguez and J. Hrbek, *J. Am. Chem. Soc.,* 2004, **126**, 8886-8887

27 J. A. Rodriguez and J. Hrbek, *Surf. Sci.,* 2010**, 604**, 241-244

28 J. A. Rodriguez, P. Liu, J. Graciani, S. D. Senanayake, D. C. Grinter, D. Stacchiola, J.Hrbek and J. Fernandez-Sanz, *J. Phys. Chem. Lett.*, 2016, **7**, 2627-2639

29 J. Kang, M. Mahapatra, N. Rui, I. Orozco, R. Shi, S. D. Senanayake and J. A. Rodriguez, *J. Chem. Phys.,* 2020, **152**, 054702

30 Z. Song, T. Cai, J. A. Rodriguez, J. Hrbek, A. S. Y. Chan and C. M. Friend, *J. Phys. Chem. B,* 2003, **107**, 1036-1043

31 Z. Song, T. Cai, Z. Chang, G. Liu, J. A. Rodriguez, J. Hrbek, *J. Am. Chem. Soc.* 2003, **125**, 8059-8066

32 P. Reinke and P. Oelhafen, *Surf. Sci*., 2000, **468**, 203-215.

33 J. A. Rodriguez, J. Dvorak and T. Jirsak, *Surf. Sci*., 2000, **457**, L413-L420.

34 T. P. St. Clair, T. Oyama, D. F. Cox, S. Otan, Y. Ishizawa, R. L. Lo, K. Fukui and Y. Iwasawa, *Surf. Sci*., 1999, **426**, 187-198.

35 S. Posada-Perez, P. J. Ramirez, J. Evans, F. Viñes, P. Liu, F. Illas and J. A. Rodriguez, *J. Am. Chem. Soc.,* 2016, **138**, 8269-8278.

36 J .A. Rodriguez , P. Liu, J. Dvorak, T. Jirsak, J. Gomes, Y. Takahashi and K. Nakamura, *J. Chem. Phys*., 2004, **121**, 465-474

37 F. Frantz and S. V. Didziulis*, Surf. Sci,*. 1998, **412/413**, 384

38S. V. Didziulis, P. Frantz, S.S. Perry, O. El-bjeirami, S. Imaduddin, P. B. Merrill, *J. Phys. Chem. B, 1999,* **103**, 11129

39 J. B. Park, J. Graciani, J. Evans, D. Stacchiola, S. Ma, P. Liu, A. Nambu, J. F. Sanz, J. Hrbek and J. A. Rodriguez, *Proc. Natl. Acad. Sci.,* 2009, **106**, 4975–4980.

40 J. A. Rodriguez, P. Liu, J. Hrbek, M. Pérez and J. Evans, *J. Mol. Catal. A: Chem.,* 2008, **281**, 59–65.

41 Y. Yang, J. Evans, J. A. Rodriguez, M. G. White and P. Liu, *Phys. Chem. Chem. Phys.,* 2010, **12**, 9909–9917.

42 J. A. Rodriguez, J. Evans, L. Feria, A. B. Vidal, P. Liu, K. Nakamura and F. Illas, *J. Catal.,* 2013, **307**, 162–169.

43 O. Lamiel, S. T. Bromley and F. Illas, *Theor. Chem. Acc*., 2013, **132**, 1312

44 J. P. Perdew, K. Burke and M. Ernzerhof, *Phys. Rev. Lett.,* 1996, **77**, 3865–3868.

45 J. R. d. S. Politi, F. Viñes, J. A. Rodriguez and F. Illas, *Phys. Chem. Chem. Phys.,* 2013, **15**, 12617-12625.

46 L. Vega, J. Ruvireta, F. Viñes and F. Illas, *J. Chem. Theory Comput.* 2018, **14**, 395-403

47 S. Grimme, J. Antony, S. Ehrlich and S. A. Krieg, *J. Chem. Phys.,* 2010, **132**, 154104.

48 G. Henkelman, B. P. Uberuaga and H. A. Jónsson, *Phys. Rev. B,* 2000, **113**, 9901–9904.

49 A. H. Larsen, J. J. Mortensen, J. Blomqvist, I. E. Castelli, R. Christensen, M. Dułak, J. Friis, M. N. Groves, B. Hammer, C. Hargus, E. D. Hermes, P. C. Jennings, P. B. Jensen, J. Kermode, J. R. Kitchin, E. L. Kolsbjerg, J. Kubal, K. Kaasbjerg, S. Lysgaard, J. B. Maronsson, T. Maxson, T. Olsen, L. Pastewka, A. Peterson, C. Rostgaard, J. Schiøtz, O. Schütt, M. K. S. Strange, T. Vegge, L. Vilhelmsen, M. Walter, Z. Zeng and K. W. Jacobsen, *J. Phys. Condens. Matter.,* 2017, **29**, 273002.

50 S. Smidstrup, A. Pedersen, K. Stokbro and H. Jónsson, *J. Chem. Phys.,* 2014, **140**, 214106.

51 G. Kresse and J. Furthmüller, *Phys. Rev. B.,* 1996, **54**, 11169–11186.

52 J. S. Yoo, J. Schumann, F. Studt, F. Abild-Pedersen and J. K. Nørskov, *J. Phys. Chem. C,* 2018, **122**, 16023−16032.

53 W. Wu, P. J. Ramirez, D. Stacchiola, and J. A. Rodriguez, *Catal. Letters,* 2014, **144**, 1418–1424.